JOURNAL OF MATERIALS SCIENCE 11 (1976) 445–457

Pressure and normal stress effects in shear yielding

J. C. M. LI, J. B. C. WU
Department of Mechanical and Aerospace Sciences, and Materials Science Program, University of Rochester, Rochester, New York, USA

The classical yielding theory of Tresca is generalized to include the effects of both hydrostatic pressure and normal stress in the slip plane. The three-parameter theory is the most general for polyhedral yield surfaces. The new theory is applied to the yielding of polystyrene. Two modes of slip: a brittle mode in the form of coarse slip bands, and a ductile mode in the form of fine slip bands, are studied separately. All three parameters are determined for each mode.

1. Introduction

Classical yielding theories (see [1]) such as the Tresca and von Mises Criteria are "one parameter" relations among the three principal stresses. The Tresca parameter is the critical shear stress and the von Mises parameter is the critical distortional strain energy. Because of their simplicity, these theories could not deal with added complications such as the effect of hydrostatic pressure.

An obvious extension or generalization of the "one parameter" theories is the "two parameter" theories. One of the earlier ones is the Coulomb or Mohr–Coulomb criterion [1] in which the critical shear stress is no longer constant but depends on the normal stress across the plane much like the sliding friction. Another is Drucker's modification [2] of Tresca and von Mises criteria in which the critical shear stress or the critical distortional strain energy depends on the hydrostatic component of stress. Although Drucker considered his modification a "proper generalization" of the Coulomb criterion, they are distinctly different. For example, in the Coulomb criterion, the direction of shear yielding is affected by the Coulomb friction. Yet in Drucker's modification of Tresca criterion, the direction of shear yielding remains that of maximum shear stress independent of the pressure coefficient.

This distinction is often not recognized and is a source of confusion in the recent literature. For example, Whitney and Andrews [3] used hydrostatic component of stress (called mean normal stress by them) in the Coulomb criterion and yet stated that the direction of yielding depends on the coefficient. Argon *et al.* [4] obviously did not attempt to differentiate between the effect of normal stress and that of pressure since they stated that the departure of shear bands from the plane of maximum shear stress can be explained by the strong pressure dependence of yielding. In fact in their Fig. 10, the σ_1–σ_2 yield envelope represents the pressure effect but the τ–σ envelope represents the effect of normal stress. This figure was reproduced by Ward [5] without clarification. Ward, too, did not attempt to differentiate between normal stress and pressure effects. In his book [1] on p. 298, the figure was mislabelled as Mohr–Coulomb yield criterion but actually it represents the pressure effect. Christiansen *et al.* [6] used a pressure term in the Mohr–Coulomb criterion and considered that as a slight modification. Matsushige *et al.* [7] considered the Coulomb criterion as a pressure modified Tresca criterion and yet used a Mohr envelope to represent the effect.

However, many authors do differentiate between the normal stress and the pressure effects. For example, Bowden and Jukes [8] examined the three possible two-parameter yield criteria, namely, the Mohr–Coulomb, the pressure modified Tresca, and the pressure modified Von Mises, and concluded that some polymers obey one and others another. Haward *et al.* [9] considered the Mohr–

Coulomb criterion and treated the pressure effect in terms of Coulomb friction. Physically the pressure modified von Mises criterion is not self consistent since it puts pressure in a different category of stress although empirically it is a valid two-parameter yield surface. This leaves only two physically sound two-parameter criteria, namely the Mohr–Coulomb and the pressure modified Tresca criteria. Although these two criteria are different, they do not have to be mutually exclusive.

For shear yielding at the microstructural level as studied in the previous paper, the Coulomb criterion is needed to understand the angular departure for the shear bands from the maximum shear stress directions. But the Coulomb criterion alone is not sufficient, since, for the fine bands which intersect at 90° indicating negligible Coulomb friction, the yield stress still depends on pressure. Thus it seems unavoidable to consider a three-parameter yield surface. These three parameters can be taken conveniently as the intrinsic Tresca shear stress, the normal stress coefficient (Coulomb friction) and the hydrostatic stress coefficient. This set of parameters define a polyhedral yield surface rather than a curved one. But it seems more physical than, for example, a relation between the three invariants of the stress tensor. It predicts also the directional properties of the shear band without further assumptions regarding plastic stress–strain relations.

The purpose of this paper is to examine the three-parameter yield surface in some detail and to present some experimental results for the determination of these parameters.

2. General shear–yield surface

For an isotropic material, a general polyhedral yield surface should have at most three parameters. This is so because the three principal stress axes can orient themselves in any direction and an equation for a plane is determined by three constants.

Following previous work but making a clear distinction between the effects of normal stress and hydrostatic stress, yielding is assumed to take place such that the following relation is satisfied:

$$|\tau| + \alpha\sigma_n + \beta\sigma_h \geqslant \tau_0. \tag{1}$$

In this relation, τ is the shear stress and σ_n is the normal stress in the plane, σ_h is the hydrostatic component of stress, and α, β, and τ_0 are constants. Since Equation 1 has three constants, it represents a general polyhedral yield surface. The quantity τ_0 is the yield stress in pure shear. Unlike the original Tresca criterion in which yielding is assumed to take place wherever the shear stress τ exceeds τ_0 in magnitude, Equation 1 now takes into consideration the effects of both σ_n and σ_h.

If the yield surface does not have planar faces, Equation 1 can be viewed as a local tangent plane so that α and β are the following slopes:

$$\alpha = -(\partial|\tau|/\partial\sigma_n)_{\sigma_h} \tag{2}$$

$$\beta = -(\partial|\tau|/\partial\sigma_h)_{\sigma_n}. \tag{3}$$

However, usually in a simple experiment, an increase in normal stress also increases the hydrostatic component simultaneously. Similarly in an experiment involving a change of hydrostatic pressure, the normal stress changes also. For these experiments, the changes of yield stress are:

$$\frac{d|\tau|}{d\sigma_n} = -\alpha - \frac{\beta}{3} \tag{4}$$

and

$$\frac{d|\tau|}{dP} = \alpha + \beta, \tag{5}$$

respectively.

In a simple tension test, the material will yield along two planes whose normals make the following angles with the tensile axis:

$$\begin{aligned}\phi_t &= \pm\tan^{-1}[\sqrt{(1+\alpha^2)} - \alpha] \\ &= \pm\tfrac{1}{2}\cot^{-1}\alpha.\end{aligned} \tag{6}$$

It is to be noted that these angles are not affected by β. The angle between the two normals encompassing the tensile axis is:

$$\theta = \cot^{-1}\alpha. \tag{7}$$

The tensile yield stress is

$$\sigma_t = 2\tau_0/[\sqrt{(1+\alpha^2)} + \alpha + \tfrac{2}{3}\beta]. \tag{8}$$

Similarly in a simple compression test, the material will yield also along two planes whose normals make the following angles with the compression axis:

$$\begin{aligned}\phi_c &= \pm\tan^{-1}[\sqrt{(1+\alpha^2)} + \alpha] \\ &= \pm\tfrac{1}{2}(\pi - \cot^{-1}\alpha).\end{aligned} \tag{9}$$

It is noted that the angle between the two normals not encompassing the compression axis is also given by Equation 7. The compressive yield stress

is (taken as positive),

$$\sigma_c = 2\tau_0/[\sqrt{(1+\alpha^2)} - \alpha - \tfrac{2}{3}\beta]. \quad (10)$$

Equations 8 and 10 show that the material has a strength differential effect [10] given by

$$\text{RSD} = 2(\alpha + \tfrac{2}{3}\beta)/\sqrt{(1+\alpha^2)}. \quad (11)$$

In a triaxial stress situation, let σ_1, σ_2 and σ_3 be the principal stresses. Consider a plane whose normal has direction cosines k_1, k_2, and k_3. Then on this plane the total stress is σ:

$$\sigma^2 = \sigma_1^2 k_1^2 + \sigma_2^2 k_2^2 + \sigma_3^2 k_3^2 \quad (12)$$

the normal stress is

$$\sigma_n = \sigma_1 k_1^2 + \sigma_2 k_2^2 + \sigma_3 k_3^2 \quad (13)$$

and hence the shear stress is τ:

$$\tau^2 = \sigma^2 - \sigma_n^2. \quad (14)$$

By definition, the hydrostatic component of stress is

$$\sigma_h = \tfrac{1}{3}(\sigma_1 + \sigma_2 + \sigma_3). \quad (15)$$

Thus yielding will occur in this plane when Equation 1 is satisfied. To see along which plane yielding is most likely to take place, the left hand side of Equation 1 can be maximized with respect to the direction cosines. It is found that for $\sigma_1 > \sigma_2 > \sigma_3$, the direction cosines are

$$k_1^2 = 1/\{1 + [\sqrt{(1+\alpha^2)} - \alpha]^2\}$$
$$k_2 = 0$$
$$k_3^2 = 1/\{1 + [\sqrt{(1+\alpha^2)} + \alpha]^2\}. \quad (16)$$

Equations 16 represent two different directions both perpendicular to the σ_2 direction. These directions make the same angles as ϕ_t given by Equation 6 with the σ_1 direction or the same angles as ϕ_c given by Equation 9 with the σ_3 direction. The angle between the two directions encompassing the σ_1 direction is also given by Equation 7.

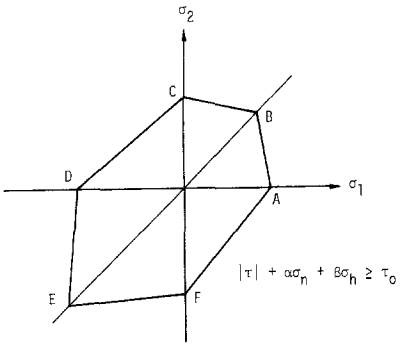

	σ_1	σ_2
A	$6\tau_0/(3\alpha_+ + 2\beta)$	0
B	$6\tau_0/(3\alpha_+ + 4\beta)$	$6\tau_0/(3\alpha_+ + 4\beta)$
C	0	$6\tau_0/(3\alpha_+ + 2\beta)$
D	$-6\tau_0/(3\alpha_- - 2\beta)$	0
E	$-6\tau_0/(3\alpha_- - 4\beta)$	$-6\tau_0/(3\alpha_- - 4\beta)$
F	0	$-6\tau_0/(3\alpha_- - 2\beta)$

$\alpha_+ = \sqrt{1+\alpha^2} + \alpha \qquad \alpha_- = \sqrt{1+\alpha^2} - \alpha$

Figure 1 Plane stress yield envelope for the three-parameter yield surface.

These direction cosines can be substituted into Equations 12 to 14 and then into Equation 1. This gives the following relation between the principal stresses:

$$\sigma_1\left[\frac{\sqrt{(1+\alpha^2)}+\alpha}{2} + \frac{\beta}{3}\right] + \sigma_2\frac{\beta}{3} - \sigma_3\left[\frac{\sqrt{(1+\alpha^2)}-\alpha}{2} - \frac{\beta}{3}\right] \geqslant \tau_0 \quad (17)$$

which is also the local yield surface. Since the three planes $\sigma_1 = \sigma_2$, $\sigma_2 = \sigma_3$, and $\sigma_3 = \sigma_1$ divide the space into six sectors each having a different order of the three principal stresses, the yield surface has

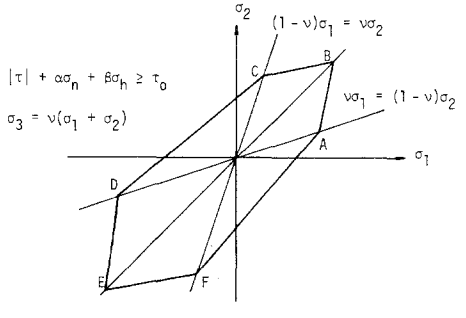

	σ_1	σ_2
A	$6(1-\nu)\tau_0/[3(1-\nu)\alpha_+ - 3\nu\alpha_- + 2(1+\nu)\beta]$	$6\nu\tau_0/[3(1-\nu)\alpha_+ - 3\nu\alpha_- + 2(1+\nu)\beta]$
B	$6\tau_0/[3\alpha_+ - 6\nu\alpha_- + 4(1+\nu)\beta]$	$6\tau_0/[3\alpha_+ - 6\nu\alpha_- + 4(1+\nu)\beta]$
C	$6\nu\tau_0/[3(1-\nu)\alpha_+ - 3\nu\alpha_- + 2(1+\nu)\beta]$	$6(1-\nu)\tau_0/[3(1-\nu)\alpha_+ - 3\nu\alpha_- + 2(1+\nu)\beta]$
D	$-6(1-\nu)\tau_0/[-3\nu\alpha_+ + 3(1-\nu)\alpha_- - 2(1+\nu)\beta]$	$-6\nu\tau_0/[-3\nu\alpha_+ + 3(1-\nu)\alpha_- - 2(1+\nu)\beta]$
E	$-6\tau_0/[-6\nu\alpha_+ + 3\alpha_- - 4(1+\nu)\beta]$	$-6\tau_0/[-6\nu\alpha_+ + 3\alpha_- - 4(1+\nu)\beta]$
F	$-6\nu\tau_0/[-3\nu\alpha_+ + 3(1-\nu)\alpha_- - 2(1+\nu)\beta]$	$-6(1-\nu)\tau_0/[-3\nu\alpha_+ + 3(1-\nu)\alpha_- - 2(1+\nu)\beta]$

$\alpha_+ = \sqrt{1+\alpha^2} + \alpha \qquad \alpha_- = \sqrt{1+\alpha^2} - \alpha$

Figure 2 Plane strain projection of the three-parameter yield surface.

six different planar faces. The intersection of the yield surface with the σ_1–σ_2 plane ($\sigma_3 = 0$) is shown in Fig. 1 and that with the plane $\sigma_3 = \nu(\sigma_1 + \sigma_2)$ (plane strain) and projected onto the σ_1–σ_2 plane is shown in Fig. 2.

In Fig. 1, the loop is symmetric with respect to the line $\sigma_1 = \sigma_2$. When $\beta = 0$, AB and ED will be parallel to σ_2 and CB and EF will be parallel to σ_1. The slope of FA is α_+/α_- and that of DC is α_-/α_+. When β increases such that

$$\beta\left(\alpha + \frac{2\beta}{3}\right) = \frac{3}{8}, \tag{18}$$

the point E moves to $-\infty$, the slopes ED and EF both become unity. When β increases further such that

$$\beta\left(\alpha + \frac{\beta}{3}\right) = \frac{3}{4} \tag{19}$$

both D and F move to $-\infty$ or DC becomes horizontal and FA becomes vertical. These effects are summarized in Fig. 3.

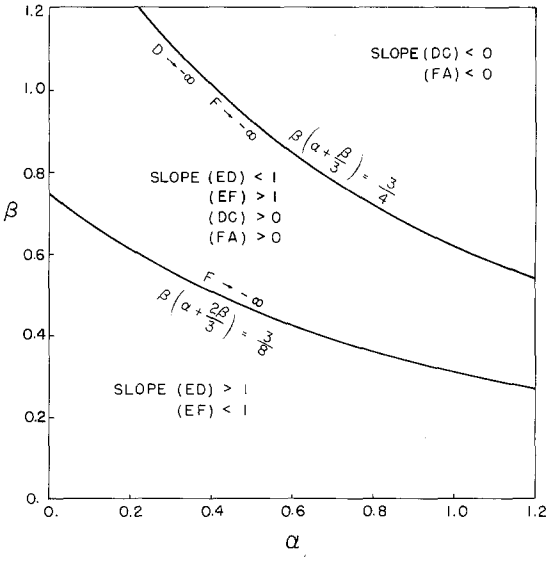

Figure 3 The effects of α and β values on Fig. 1.

In Fig. 2, the loop becomes identical to that of Fig. 1 when $\nu = 0$. For $\nu = 0.5$, the loop becomes open with A, B, and C merging into one point at

$$\sigma_1 = \sigma_2 = \tau_0/(\alpha + \beta). \tag{20}$$

The slope DC becomes $[\sqrt{(1+\alpha^2)} - \alpha - \beta]/[\sqrt{(1+\alpha^2)} + \alpha + \beta]$ and the slope FA becomes the reciprocal of that. The points D and F have gone to $-\infty$. For other ν values, the loop opens when the point E moves to $-\infty$ at

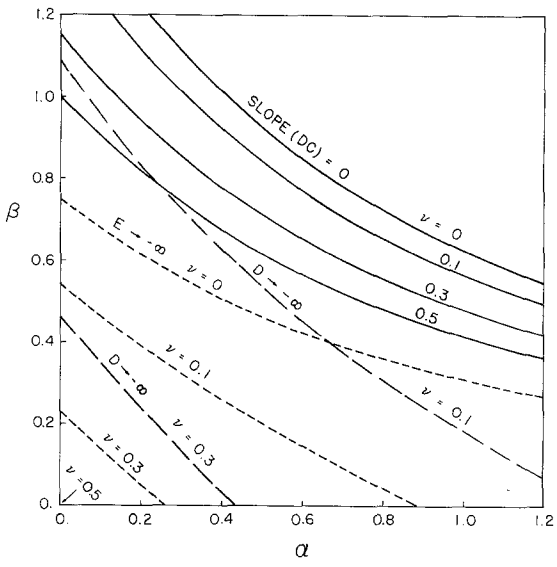

Figure 4 The effects of α, β and ν values on Fig. 2.

$$\beta = 3[(1-2\nu)\sqrt{(1+\alpha^2)} - (1+2\nu)\alpha]/4(1+\nu). \tag{21}$$

Equation 21 is plotted in Fig. 4 for $\nu = 0, 0.1, 0.3$, and 0.5. At $\nu = 0.5$ the line becomes $\alpha + \beta = 0$ and hence the loop is open at any positive α, β values. The loop opens more when D and F move to $-\infty$. This happens when

$$\beta = [3(1-2\nu)\sqrt{(1+\alpha^2)} - 3\alpha]/2(1+\nu). \tag{22}$$

Equation 22 is plotted also in Fig. 4 for $\nu = 0$, 0.1, 0.3, and 0.5. The curve for $\nu = 0$ is the same as the one for slope DC = 0 and that for $\nu = 0.5$ is again $\alpha + \beta = 0$. The loop opens further when the slope of DC becomes zero or that of FA becomes infinite. This happens when

$$3[\sqrt{(1+\alpha^2)} - \alpha] = 2(1+\nu)\beta. \tag{23}$$

Equation 23 is plotted also in Fig. 4 for $\nu = 0$, 0.1, 0.3, and 0.5. It is seen that for plane strain compression, yielding is in general more difficult than for plane stress compression.

Fig. 2 shows also that in a tension test, the yield stress for plane strain is

$$\sigma_t = 2\tau_0/\left[\sqrt{(1+\alpha^2)} + \alpha + \frac{2(1+\nu)}{3}\beta\right] \tag{24}$$

and similarly the yield stress in compression is (taken as positive)

$$\sigma_c = 2\tau_0/\left[\sqrt{(1+\alpha^2)} - \alpha - \frac{2(1+\nu)}{3}\beta\right]. \tag{25}$$

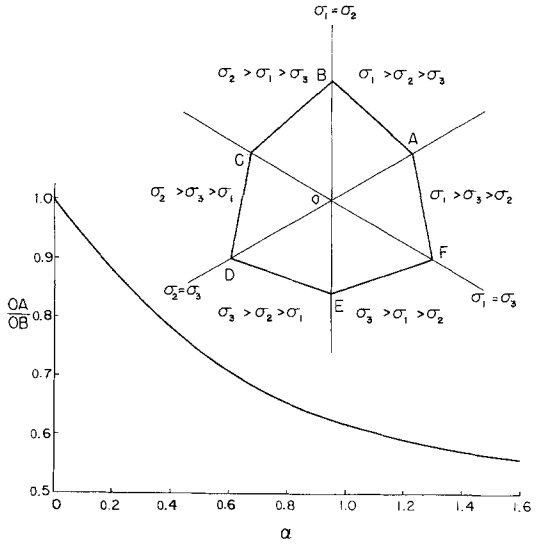

Figure 5 Cross-section of yield surface on a (1 1 1) plane.

These relations give the following relative strength differential effect [10]:

$$\mathrm{RSD} = 2\left[\alpha + \frac{2(1+\nu)}{3}\beta\right]/\sqrt{(1+\alpha^2)}. \quad (26)$$

This effect is seen to be slightly different from that given by Equation 11 for plane stress.

Since the yield surface has a three-fold symmetry around the [1 1 1] direction, it is interesting to look at a section cut by an octahedral plane of constant σ_h. This is shown in Fig. 5. It is not a regular hexagon although all the sides are equal to

$$\overline{AB} = 6\sqrt{2}[\tau_0 - (\alpha+\beta)\sigma_h] \times \sqrt{(3+4\alpha^2)/(9+8\alpha^2)}. \quad (27)$$

Owing to the three-fold symmetry, the lengths $\overline{OA}$, $\overline{OC}$ and $\overline{OE}$ are equal and are:

$$\overline{OA} = 2\sqrt{6}[\tau_0 - (\alpha+\beta)\sigma_h]/[3\sqrt{(1+\alpha^2)}+\alpha]. \quad (28)$$

Similarly, the lengths $\overline{OB}$, $\overline{OD}$ and $\overline{OF}$ are equal. The ratio between them is

$$\overline{OA}/\overline{OB} = [3\sqrt{(1+\alpha^2)}-\alpha]/[3\sqrt{(1+\alpha^2)}+\alpha] \quad (29)$$

which is shown in Fig. 5. It is seen that all these dimensions become zero at

$$\sigma_h = \tau_0/(\alpha+\beta). \quad (30)$$

In other words, the yield surface is a hexagonal pyramid. This is true even when α or β is zero. However, when β is zero, the pyramid becomes regular.

3. Experiments on polystyrene

3.1. Two distinct shear processes

It is well known that when crazing is suppressed, amorphous polymers such as polystyrene deform by localized shear with the appearance of intense shear bands [11]. More recently Bowden and Raha [12] and Kramer [13] reported what appeared in the optical microscope "diffuse" shear zones which sometimes accompany the intense shear bands. A careful study of the diffuse shear zones (see previous paper) using electron microscopy revealed numerous, discontinuous, less well-defined but nevertheless distinct fine shear bands usually appeared in two sets intersecting at nearly right angles. An example is shown in Fig. 6. Obviously there are two shear processes in the deformation of polystyrene, a "coarse band" process and a "fine band" process. Besides the difference in their appearances, the coarse band propagates fast and along a localized path, inclines at more than 45° with the tension axis or less than 45° with the compression axis, and invariably produces shear fracture when it propagates across the specimen. On the other hand, the fine bands spread by

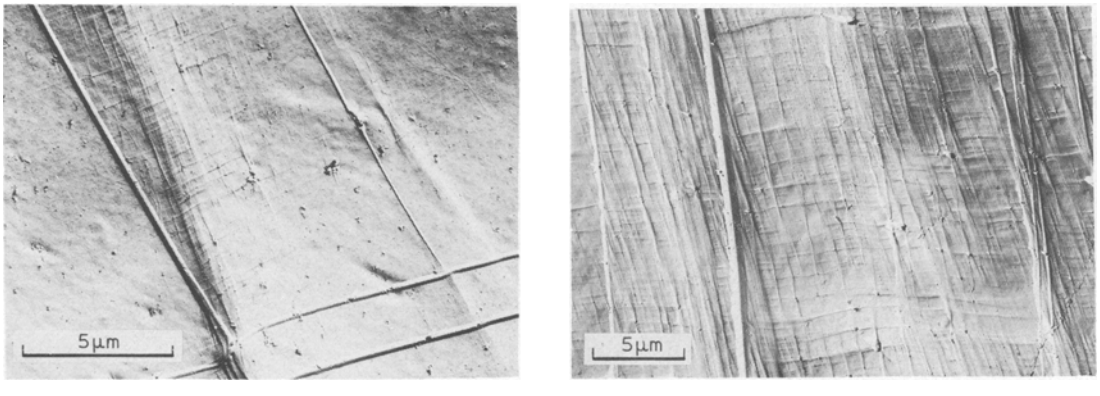

Figure 6 Coarse and fine slip bands viewed in the electron microscope.

multiplication mainly along the maximum shear stress direction, contribute largely to the macroscopic strain and cause shape changes of the specimen, but do not induce shear fracture. Hence the "coarse band" process is also a brittle mode and the "fine band" process a ductile mode. There are ways to change the relative abundance of these deformation modes. For example, furnace cooled specimens favour the brittle mode while quenched specimens favour the ductile mode. These findings are discussed in the preceding paper. The following experiments were designed to estimate the three parameters, α, β, and τ_0 in the yield criterion, Equation 1, for each of the two shear processes.

3.2. Material preparation

Atactic polystyrene available commercially from Westlake Co in the form of sheets 0.25 in. thick was cut into blocks of proper sizes and annealed at 115° C for 20 h. The annealed blocks were either furnace cooled for the study of coarse bands or quenched in liquid nitrogen for the study of fine bands. Specimens were then machined from these blocks and polished to 0.05 μm alumina finish.

From gel permeation chromatography, the weight-average molecular weight is 599 000 and the number-average is 348 000. The glass transition temperature was determined to be 101° C by differential scanning calorimetry.

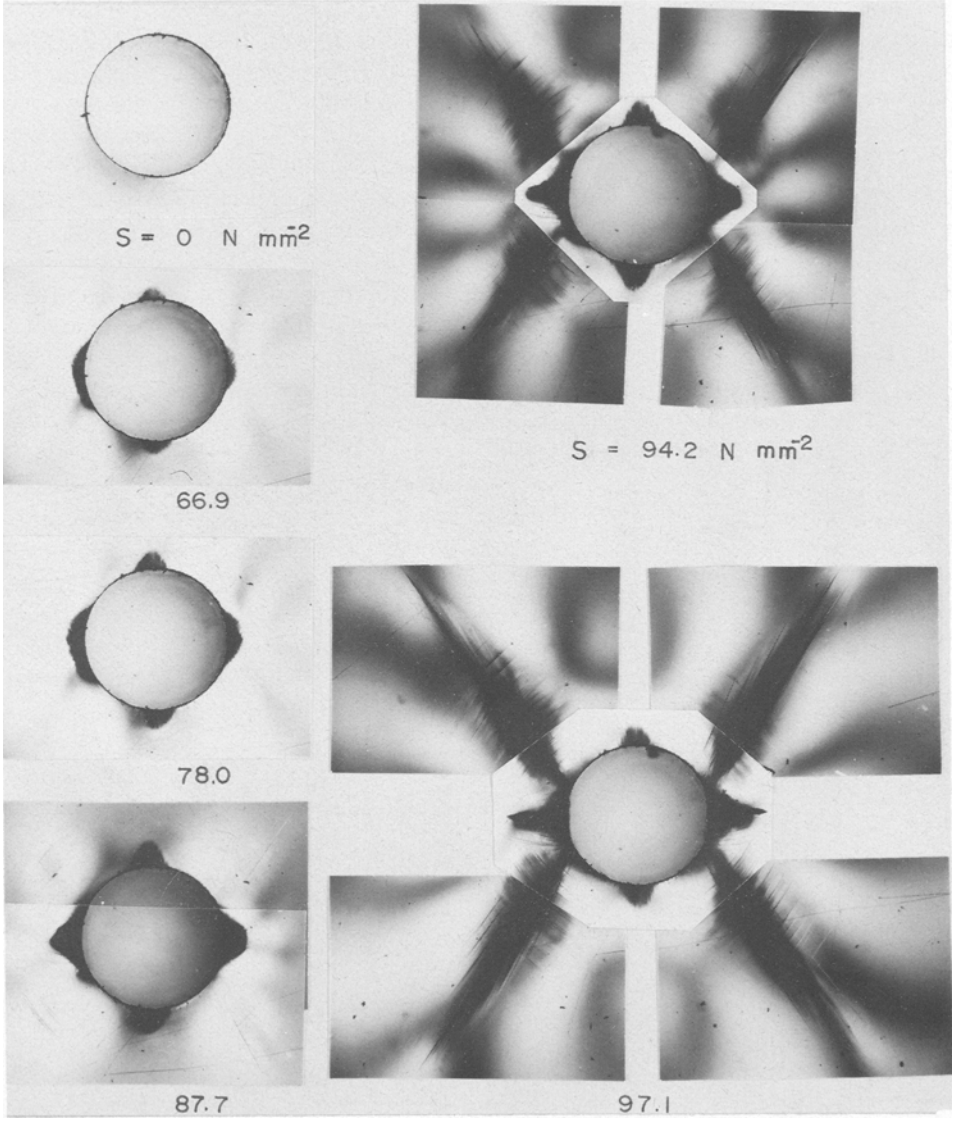

Figure 7 The initiation of coarse bands around a hole under compression.

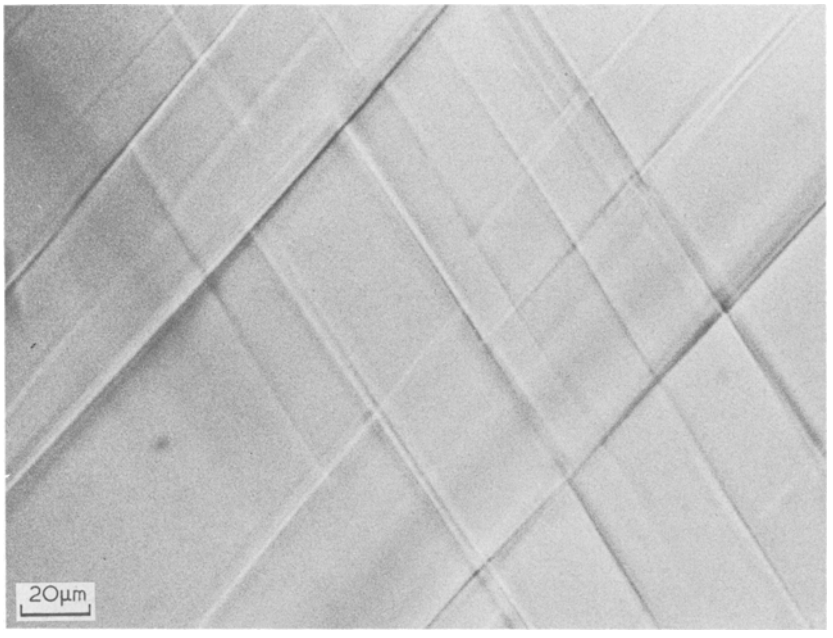

Figure 8 Details of one of the band packets in Fig. 7 showing the numerous intersections of coarse bands.

3.3. The determination of α

Based on the three-parameter theory of the yield surface just presented, the parameter α can be determined directly from the angle at the intersection of slip bands by using Equation 7.

For the study of coarse bands a hole of 0.11 cm diameter was drilled through the thickness at the centre of a 2 cm x 2 cm square specimen (0.25 in. thick). The stress concentration was needed to facilitate production of coarse bands and reduce the interference of fine bands. Fig. 7 shows the successive stages of the appearance of coarse bands when the specimen is compressed along one of its sides at different stresses. It is seen that when four band packets are fully developed, numerous intersections can be seen as enlarged in Fig. 8. The angles of these intersections were measured from such optical micrographs and the α's calculated by Equation 7. Some corrections were made because of the fact that these micrographs are taken on unloaded specimens. Since the coarse bands do not produce much plastic strain, the total compressive strain is nearly all elastic and recoverable. The correction amounted to about 3° using the following equation:

$$\frac{\alpha_{\text{corr}}}{\alpha} = \frac{1 + m_1 m_2 \xi^2}{(1 + m_1 m_2)\xi} \qquad (31)$$

where $\xi = (1 - \epsilon)/(1 + \nu\epsilon)$, ϵ is the recovered strain (taken as positive), and m_1, m_2 are the observed slopes of the intersecting bands when compression is along the y-axis. The corrected angle was found to be $79 \pm 1°$ at room temperature corresponding to $\alpha = 0.19 \pm 0.02$. The results are plotted as a function of temperature in Fig. 9. Temperatures other than room temperature were achieved by testing in the Instron environment chamber. The strain-rate used for compression was always 0.005 sec^{-1}.

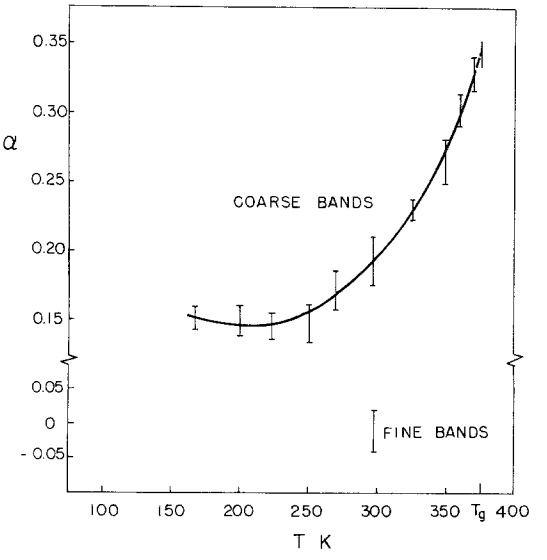

Figure 9 The α values for slip bands in polystyrene as a function of temperature.

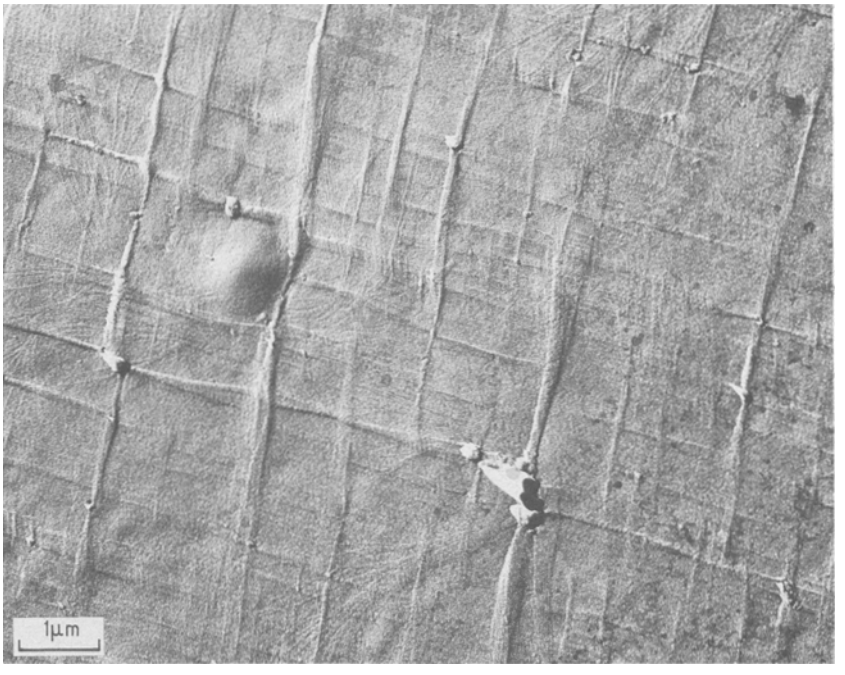

Figure 10 Electron micrograph of platinum-carbon replica of deformed surface showing the intersection of fine bands in polystyrene.

The room temperature angle of $79 \pm 1^\circ$ can be compared with previous results. Argon *et al.* [4] measured the angle between the compression axis and the band packet presumably at the relaxed state. They reported such angle to be 38° corresponding to our angle of 76°. Kramer [13] measured the same angle under static loading at the strained condition and reported $38.1 \pm 0.5^\circ$ corresponding to ours of $76.2 \pm 1^\circ$. Bowden and Jukes [8] did plane strain compression and reported a value corresponding to ours of 80° after correction of recovered strain. In view of the different testing conditions, the agreement seems satisfactory.

For the study of fine bands, specimens furnace cooled or quenched into liquid nitrogen were deformed at room temperature using several strain-rates. Platinum–carbon replicas were made from the surface of deformed specimens. A typical electron micrograph is shown in Fig. 10. Here again since the replicas were made on unloaded specimens, the angle of intersection of the two bands had to be corrected for recoverable strain as in the case of coarse bands. However, an additional correction was needed here because of the fact that fine bands produced plastic strain. The angle between the intersecting fine bands encompassing the compression axis had increased during deformation. At the time of observation, the angle was larger than when they began to appear. This correction depended on plastic strain and was opposite to the other correction. After these two corrections, the angle was found close to 90° independent of strain-rates. This angle agrees with Kramer's observation [13] that his "diffuse zone" in polystyrene tends to propagate along maximum shear directions. Our results for fine bands are shown also in Fig. 9.

3.4. The determination of β

For the determination of β, it was found convenient to load the specimen with a narrow smooth punch. The elastic problem is a classical one and the solution depends on the boundary condition assumed. As shown in Fig. 11, when the punch is pressed onto the specimen, two possibilities represent the extremes: the first is when the punch is very hard compared to the specimen so that the displacement under the punch is constant. This solution involves two singularities at the corners of the punch and hence the elastic field is more complex. The other is when the punch is soft compared to the specimen so that the stress is constant under the punch. No singularities appear at the corners and hence the elastic field is simpler. However, the two solutions ap-

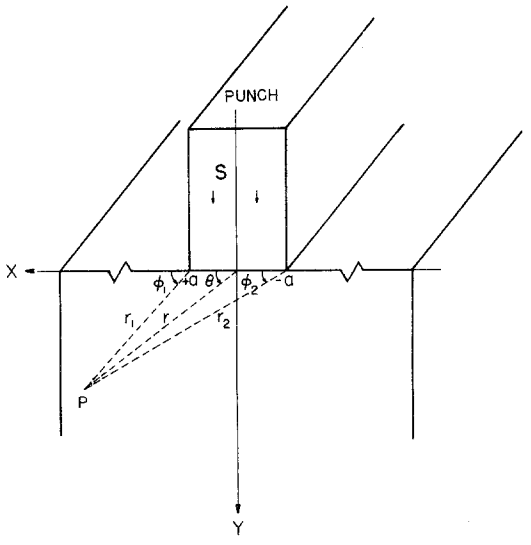

$$\sigma_{xx} = -\frac{S}{2\pi}\left[2(\phi_1 - \phi_2) + \sin 2\phi_1 - \sin 2\phi_2\right]$$

$$\sigma_{yy} = -\frac{S}{2\pi}\left[2(\phi_1 - \phi_2) - \sin 2\phi_1 + \sin 2\phi_2\right]$$

$$\sigma_{xy} = \frac{S}{2\pi}\left[\cos 2\phi_1 - \cos 2\phi_2\right]$$

Figure 11 Elastic stress fields under a narrow smooth punch.

proach each other at distances larger than the width of the punch. For simplicity, the latter solution is used. The stress field is shown in Fig. 11. For plane strain, $\sigma_{zz} = \nu(\sigma_{xx} + \sigma_{yy})$ and for plane stress, $\sigma_{zz} = 0$. All other components of stress are zero.

Based on this stress field, the maximum shear stress in planes parallel to the z-axis is

$$\tau_{\max} = (s/\pi)\sin\phi \qquad (32)$$

where $\phi = \phi_1 - \phi_2$. The other two principal shear stresses are, in the case of plane stress:

$$\tau_{\max} = (s/2\pi)(\phi \pm \sin\phi) \qquad (33)$$

and in the case of plane strain:

$$\tau_{\max} = (s/2\pi)[(1-2\nu)\phi \pm \sin\phi]. \qquad (34)$$

It is seen that the contours for these stresses are all circles passing through the corners of the punch. These circles are then the yield loci for $\alpha = \beta = 0$. It can be shown that the yield loci are still circles even when α and β are not zero.

Thus it is only necessary to examine the situation along the y-axis. In units of s/π, $\sigma_{xx} = -\phi + \sin\phi$, $\sigma_{yy} = -\phi - \sin\phi$ and $\sigma_{zz} = 0$ for plane stress and $-2\nu\phi$ for plane strain. Hence for plane stress, $\sigma_{zz} > \sigma_{xx} > \sigma_{yy}$, the yield condition Equation 17 becomes:

$$(3\alpha_- - 4\beta)\phi + 3\alpha_- \sin\phi \geqslant 6\tau_0\pi/s. \qquad (35)$$

Equation 35 is in the form of

$$A\phi \pm \sin\phi \geqslant B. \qquad (36)$$

For $|A| < 1$ and the + sign, the left-hand side has a maximum at $\cos\phi = -A$ or at $y^2/a^2 = (1-A)/(1+A)$. For $A > 1$ and either sign or for $A > 0$ and the $-$ sign, the left-hand side is largest at $\phi = \pi$ or $y = 0$. For $A < -1$ and either sign or for $A < 0$ and the $-$sign, the largest value is zero at $\phi = 0$ or $y \to \infty$. These properties and the largest values are shown in Fig. 12. It is seen that when β is within a range of values such that yielding takes place at a finite y which can be measured, β can be calculated from such measurements.

When Equation 35 is satisfied, a bulge parallel to x would appear on the surface. Upon increasing load, slip in other planes may occur. These are shown in Table I for both plane stress and plane strain. It is seen that the yield conditions are all of the general form of Equation 36. In the case of

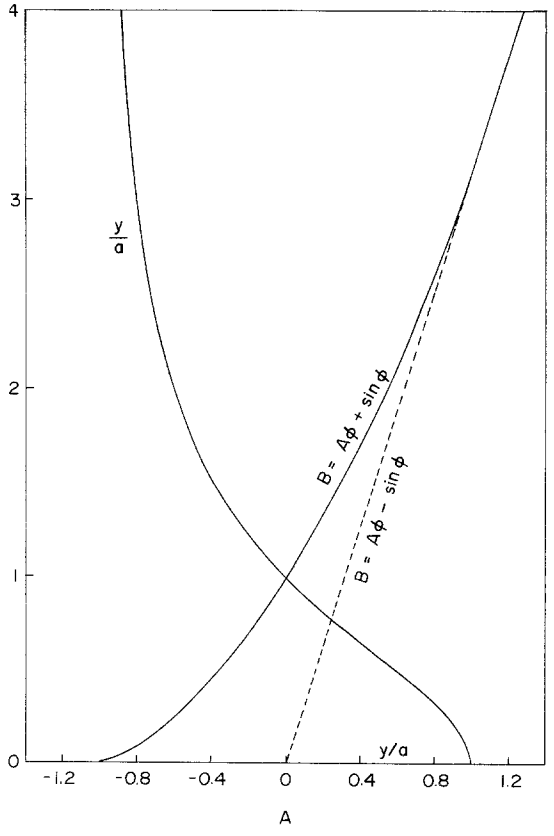

Figure 12 The maximum values for the function $B = A\phi \pm \sin\phi$.

TABLE I Yielding under a smooth flat punch of uniform stress

(a) Plane stress: $\sigma_{xx} = (s/\pi)(\sin\phi - \phi)$, $\sigma_{yy} = -(s/\pi)(\sin\phi + \phi)$, $\sigma_{zz} = 0$

Yield condition	Surface appearance
$(3\alpha_- - 4\beta)\phi + 3\alpha_- \sin\phi = 6\tau_0\pi/s$	bulge in x
$(3\alpha_- - 4\beta)\phi - 3\alpha_- \sin\phi = 6\tau_0\pi/s$	bulge in y
$-(3\alpha + 2\beta)\phi + 3\sqrt{(1+\alpha^2)}\sin\phi = 3\tau_0\pi/s$	shear

(b) Plane strain: $\sigma_{xx} = (s/\pi)(\sin\phi - \phi)$, $\sigma_{yy} = -(s/\pi)(\sin\phi + \phi)$, $\sigma_{zz} = -2\nu\phi(s/\pi)$

Yield condition	Surface appearance
$[3\alpha_- - 6\nu\alpha_+ - 4(1+\nu)\beta]\phi + 3\alpha_- \sin\phi = 6\tau_0\pi/s$	bulge in x
$[-3\alpha_+ + 6\nu\alpha_- - 4(1+\nu)\beta] + 3\alpha_+ \sin\phi = 6\tau_0\pi/s$	bulge in y (small ϕ)
$[3\alpha_- - 6\nu\alpha_+ - 4(1+\nu)\beta]\phi - 3\alpha_- \sin\phi = 6\tau_0\pi/s$	bulge in y (large ϕ)
$-[3\alpha + 2(1+\nu)\beta]\phi + 3\sqrt{(1+\alpha^2)}\sin\phi = 3\tau_0\pi/s$	shear

plane strain, $\sigma_{xx} > \sigma_{zz} > \sigma_{yy}$ for small ϕ and $\sigma_{zz} > \sigma_{xx} > \sigma_{yy}$ for large ϕ. The demarcation ϕ is when $\sin\phi/\phi = 1 - 2\nu$.

Steel punches of two sizes, 1.43 and 3.33 mm were pressed onto one side of the 2 x 2 cm^2 specimen in the Instron. A piece of teflon tape was inserted between the punch and the specimen to ensure the boundary condition of constant stress under the punch. The cross head of the Instron was lowered at the rate of 0.1 mm sec^{-1} and was to reverse its motion immediately when a preset load had reached. Plane strain condition was fulfilled by clamping two specimens together in the thickness dimension so that the total thickness is unchanged during compression. Plane stress condition was difficult to fulfill and was not used.

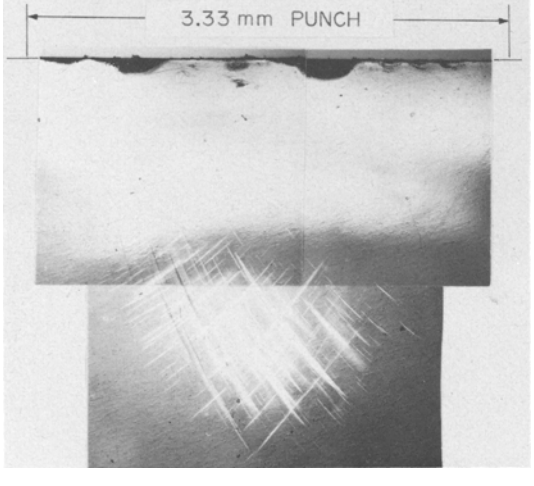

Figure 13 Optical micrograph of coarse bands appeared under a punch.

Coarse bands can be easily seen in the optical microscope. They appear to initiate near the y-axis as shown in Fig. 13. No detectable deformation under the punch is observable since the coarse bands contribute little to macroscopic strain. From the location of these bands, β can be calculated as summarized in Table II. It is seen that the values are consistently negative. When the α and β values are substituted into the four yielding conditions for plane strain in Table I, the shear appearance (for slip on planes parallel to z) requires the least load confirming the observed shear bands. On the optical micrograph, two circles can be drawn passing through the corners of the punch and defining the boundaries of the yield region. These two circles should have the same τ_0/s from which τ_0 can be determined. This is recorded also in Table II.

Fine bands cannot be easily seen in the optical microscope. However, they can be revealed by etching with a mixture of chromic and sulphuric acids. A typical optical micrograph is shown in

TABLE II Determination of β and τ_0 by observing yielding under a punch

Mode of yielding	Punch size $2a$ (mm)	y_1/a	y_2/a	Band appearance	β	Load (N)	τ_0 (N mm^{-2})
coarse bands	1.43	0.531	1.930	shear	−.216	186.5	48.8
		0.615	1.678	shear	−.212	185.5	52.1
	3.33	0.661	1.562	shear	−.211	160.6	46.4
		0.781	1.363	shear	−.192	155.2	46.4
fine bands	1.43	0.909	1.497	shear	.172	185.8	45.7
		1.035	1.301	shear	.172	190.4	45.5

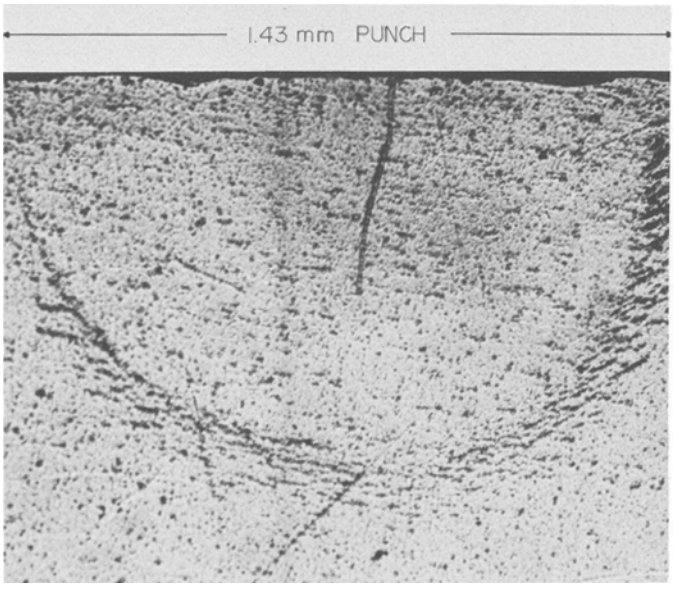

Figure 14 Optical micrograph of fine bands developed under a punch as revealed by etching.

Fig. 14. Measurements on these graphs enable determination of β and τ_0 as just described. They are summarized also in Table II. Since the fine bands are main contributors to plastic strain, the value of 0.172 for β can be compared with literature values on macroscopic yielding experiments under hydrostatic pressure. By taking our value of α, namely, 0.0, Equation 5 shows that β gives directly the pressure coefficient of shear yield stress. The measurements of Pugh *et al.* [14] are calculated by Christiansen *et al.* [6] to yield a value of 0.058. Christiansen *et al.* themselves obtained a value of 0.089. On the other hand, Whitney and Andrews [3] found a value of 0.23 and Bowden and Jukes [8] reported a value of 0.25. The average of the four values is 0.16 which compares reasonably well with our 0.17. The reason behind the diversity of these values is unknown at present.

3.5. The determination of τ_0

In addition to the determination of τ_0 under the punch, τ_0 can be determined also by examining Fig. 7. The stress field around a small hole in an infinite medium is well known and is shown in Fig. 15 for plane strain. For plane stress, σ_{zz} is simply zero. Since shear bands are observed, the yield condition, Equation 17, becomes

$$\sqrt{(1+\alpha^2)}\sqrt{\left[\left(\frac{\sigma_{rr}-\sigma_{\theta\theta}}{2}\right)^2+\sigma_{r\theta}^2\right]}+(\sigma_{rr}+\sigma_{\theta\theta}+\sigma_{zz})\left(\frac{\alpha}{2}+\frac{\beta}{3}\right)\geqslant\tau_0 \quad (37)$$

where σ_{rr}, $\sigma_{\theta\theta}$, σ_{zz}, and $\sigma_{r\theta}$ are shown in Fig. 15.

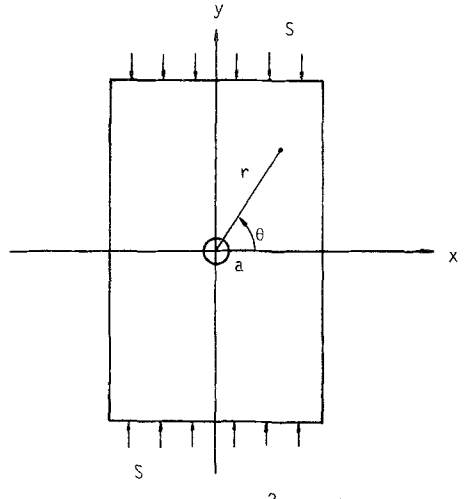

Figure 15 The stress field around a small hole in an infinite medium under compression.

Equation 37 with the equality sign is plotted in Fig. 16 for coarse bands using $\alpha = 0.194$ and $\beta = -0.21$. These yield loci can be compared with pictures such as Fig. 7 to obtain τ_0. The estimated values of τ_0 as a function of temperature are shown in Fig. 17.

For fine bands, τ_0 can be calculated directly from compressive yield stress on unnotched specimens because plastic strain is contributed mostly

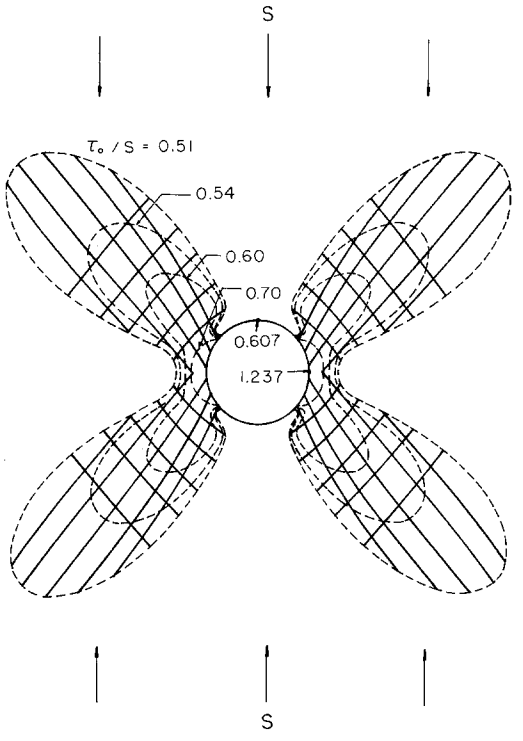

Figure 16 The theoretical yield loci for coarse bands around a small hole under compression. (-------- stress; ——— direction.)

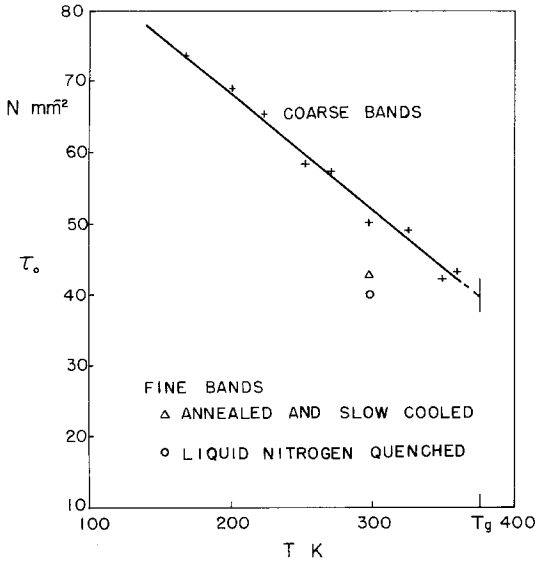

Figure 17 The instrinic Tresca stress for coarse and fine bands in polystyrene as a function of temperature ($\dot{\epsilon} = 0.005\ \text{sec}^{-1}$).

by fine bands. By using Equation 10 and knowing α and β, τ_0 can be calculated as shown also in Fig. 17. It is seen that τ_0 for annealed and slow-cooled specimens are consistently larger than that for liquid nitrogen quenched specimens. This may arise from the possibility that quenching introduces more sources for fine band generation.

3.6. The yield surfaces for polystyrene

With all three parameters determined for each mode of yielding as shown in Table III at room temperature, we can construct the projection of these yield surfaces onto a co-ordinate plane as shown in Figs. 18 and 19. An outstanding feature

TABLE III Yielding parameters for both coarse and fine bands. $|\tau| + \alpha\sigma_n + \beta\sigma_h \geqslant \tau_0$

	α	β	τ_0 (N mm^{-2})
Coarse bands	0.19	−0.21	52
Fine bands	0.0	0.17	43

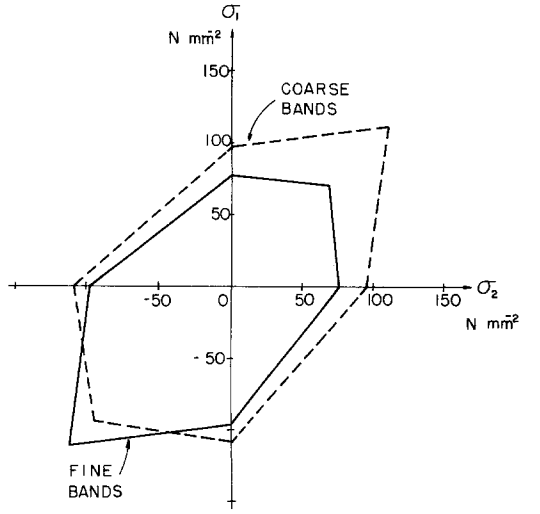

Figure 18 Plane stress yield envelope for both coarse and fine bands in polystyrene ($\dot{\epsilon} = 0.005\ \text{sec}^{-1}$).

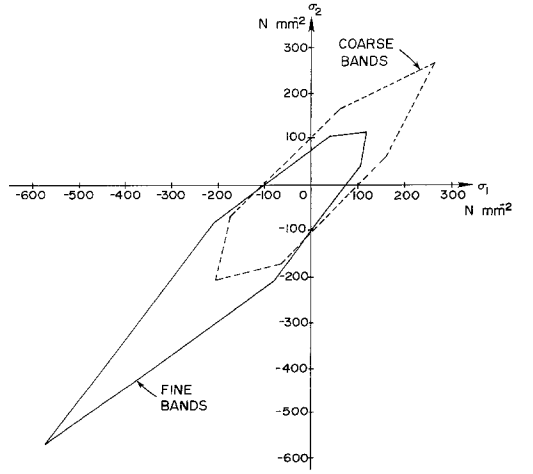

Figure 19 Plane strain yield projection for both coarse and fine bands in polystyrene ($\dot{\epsilon} = 0.005\ \text{sec}^{-1}$).

is that under tension (without crazing) fine bands require less stress than coarse bands and similarly under compression. Since coarse bands do not contribute much to plastic strain but do induce shear fracture, it is expected that under hydrostatic pressure a polymer such as polystyrene may have a higher yield stress but lower ductility in compression or when crazing is suppressed. An example is PTFE as reported by Sauer *et al.* [15], Christiansen *et al.* [6], and Davis and Pampillo [16]. Although there may be other factors, two yielding modes with different pressure effects may play an important role in such behaviour.

4. Summary and conclusions

(1) A three-parameter polyhedral yield surface is proposed. These three parameters are the intrinsic Tresca shear stress, the normal stress coefficient (Coulomb friction), and the hydrostatic stress effect.

(2) The properties of such yield surfaces are studied in some detail. Behaviour under simple tension and compression, hydrostatic pressure, and general triaxial stress conditions are discussed. The strength differential effect is expressed in terms of the yielding parameters.

(3) Polystyrene was chosen to apply the theory because of its easily observable shear bands. Two distinct shear modes are differentiated and their yield behaviour studied separately.

(4) The normal stress coefficient is determined by the angle between shear bands. The hydrostatic stress effect is determined by the location of yielding under a narrow smooth flat punch. The latter experiment yields also the intrinsic Tresca stress. The yield behaviour around a hole is used also to determine the yield parameters.

(5) The yield parameters for both shear modes are shown in Table III for room temperature. The yield surfaces corresponding to these parameters are shown in Figs. 18 and 19. Some temperature effects are shown in Figs. 9 and 17.

(6) The increased yield stress and decreased ductility for some polymers under hydrostatic pressure may arise from two yielding modes with different pressure effects such as those reported here for polystyrene.

Acknowledgements

The molecular weights and the glass transition temperature for the polystyrene used were kindly determined for us by S.E.B. Petrie and A.L. Spatorico of Eastman Kodak Co. This research was partially supported by the Army Research Office, Durham, North Carolina through contract DA-ARO-D-31-124-73-G77.

References

1. I. M. WARD, "Mechanical Properties of Solid Polymers" (John Wiley, London, 1971) p. 281.
2. D. C. DRUCKER, *J. Mech. Phys. Solids* **1** (1953) 217. See also D. C. DRUCKER and W. PRAGER, *Qu. Appl. Math.* **10** (1952) 157.
3. W. WHITNEY and R. D. ANDREWS, *J. Polymer Sci. C* **16** (1967) 2981.
4. A. S. ARGON, R. D. ANDREWS, J. A. GODRICK and W. WHITNEY, *J. Appl. Phys.* **39** (1968) 1899.
5. I. M. WARD, *J. Polymer Soc. C* **32** (1971) 195.
6. A. W. CHRISTIANSEN, E. BAER and S. V. RADCLIFFE, *Phil. Mag.* **24** (1971) 451.
7. K. MATSUSHIGE, S. V. RADCLIFFE and E. BAER, *J. Mater. Sci.* **10** (1975) 833.
8. P. B. BOWDEN and J. A. JUKES, *ibid* 7 (1972) 52.
9. R. N. HAWARD, B. M. MURPHY and E. F. T. WHITE, *J. Polymer. Sci. A-2* **9** (1971) 801.
10. C. A. PAMPILLO, L. A. DAVIS and J. C. M. LI, *Scripta Met.* **6** (1972) 765.
11. W. WHITNEY, *J. Appl. Phys.* **34** (1963) 3633.
12. P. B. BOWDEN and S. RAHA, *Phil. Mag.* **22** (1970) 463.
13. E. J. KRAMER, *J. Macromol. Sci.-Phys.* **B10** (1974) 191.
14. H. Ll. D. PUGH, E. F. CHANDLER, L. HOLLIDAY and J. MANN, *Polymer Eng. Sci.* **11** (1971) 463.
15. J. A. SAUER, D. R. MEARS and K. D. PAE, *Europ. Polymer J.* **6** (1970) 1015.
16. L. A. DAVIS and C. A. PAMPILLO, *J. Appl. Phys.* **43** (1972) 4285.

Received 9 July and accepted 29 July 1975.